Aggregation Mechanism of Nanoslabs with Zeolite MFI-Type Structure

C. E. A. Kirschhock, R. Ravishankar, P. A. Jacobs, and J. A. Martens*

Center for Surface Chemistry and Catalysis, K.U. Leuven, Kardinaal Mercierlaan 92, B-3001 Heverlee, Belgium

Received: July 1, 1999; In Final Form: October 11, 1999

The transformation of a suspension of MFI nanoslabs into colloidal Silicalite-1 at 373 K was monitored with in situ low angle and wide angle X-ray scattering (XRS). The low angle region of the diffractograms taken in the course of the crystallization could be fitted by 1 to 3 Lorentzian lines, representing 1 to 3 populations of particles with different sizes corresponding to nanoslabs, intermediates, and large particles. The large particles gave rise to the Bragg diffraction characteristic of Silicalite-1 zeolite. The measured X-ray data at low angles were at all times in agreement with the presence of entities that are multiples of the nanoslab, measuring 1.3 × 4 × 4 nm. The crystallization was performed in an open vessel with reflux cooler, and in a closed container. In both conditions, a consecutive conversion pattern of nanoblocks into intermediates into large particles was observed. The evolution of volume populations can be fitted with first-order reaction kinetics for the conversion of the nanoslab volume into intermediates and an autocatalytic conversion of intermediates into large particles. This aggregation mechanism is supported by the interaction potentials of the different faces of the nanoslabs decorated with tetrapropylammonium cations, estimated using extended DLVO theory. The proposed mechanism can account for the nature of the intermediates, the preferential growth of Silicalite-1 in the crystallographic "*c*" direction, the strain in the colloidal Silicalite-1 crystals in the crystallographic "*a*" direction, and the influence of reaction conditions on the crystallization kinetics.

Introduction

The formation of a suspension of subcolloidal Silicalite-1 particles from tetraethyl orthosilicate (TEOS) and aqueous tetrapropylammonium hydroxide (TPA−OH) solution proceeds through a series of discrete molecular steps, which were previously identified with ^{29}Si NMR, XRS, GPC, and IR.[1−3] The first silicon condensations lead to the formation of the bicyclic pentamer, the pentacyclic octamer, and the tetracyclic undecamer, having a concave hydrophobic silica surface interacting with a propyl group of TPA and a convex hydrophilic outer surface interacting with the aqueous solution. Three tetracyclic undecamers, each interacting with one propyl group of a TPA cation, condense into a 33 Si atom containing precursor that is unique to the MFI framework connectivity and is occluding the TPA. At room temperature, the precursors condense with each other to form larger species. First, there is a linking of three precursors along the later crystallographic "*c*" direction of MFI, followed by a coupling of four of such units along "*b*". This linking of twelve precursors finally results in the formation of nanoslabs with dimensions of 1.3 nm in the "*a*" direction and 4.0 nm in the "*b*" and "*c*" crystallographic directions of the Silicalite-1 framework.[1] These nanoslabs were identified with the subcolloidal Silicalite-1 particles present during the formation of MFI type zeolite, which have been observed many times in gels and clear solutions.[4−10]

A previously proposed molecular model for MFI zeolite formation, involving condensation of double five rings, led to MFI materials with missing framework sites.[11] The sequences of successive aggregations starting with the precursor first to nanoblocks, then to intermediately sized particles and finally, after heating, to the product colloidal Silicalite-1 do not lead to missing framework silicon atoms.[1−3] Neither is there a need for rearrangements of the silicon atoms in the aggregating species.

The yield on silicon basis of nanoslabs in a mixture with chemical composition corresponding to the molar ratios 5 SiO_2: 20 ethanol:30 H_2O:1 TPA_2O at room temperature is ca. 70%.[3] The remaining silicon is present in aggregates of the nanoslabs representing specific structures, built from square tablets of 2 × 2 nanoslabs coupled via their "*ab*" and "*ac*" faces, and with dimensions of 1.3 × 8 × 8 nm. These square tablets are stacked in the "*a*" direction. The largest stack observed at room temperature was twelve tablets thick and has dimensions of 15.6 × 8 × 8 nm.[3] Upon heating to 373 K, the clear suspension of nanoslabs gives rise to the formation of a colloidal suspension of Silicalite-1 particles with dimensions in the range from 18 to 100 nm.[4,6−8,10,12]

The present work is concerned with the role that the nanoslabs and the intermediates play in the formation of colloidal Silicalite-1. In situ low angle and wide angle X-ray scattering (XRS) were used to shed light on the fate of the nanoslabs and intermediates during the crystallization process. The experiments are in favor of an aggregation type of crystallization mechanism, in contradiction to the recently proposed dissolution and growth model.[4] This discrepancy is addressed by estimation of the potential energy of the nanoslab surfaces as a function of the interparticle distance using extended DLVO theory and a precise description of these surfaces gained in previous work.[1−3]

Experimental Section

The nanoslab suspension was prepared by mixing of 10 mL of tetraethyl orthosilicate (TEOS; Acros 98%) with 9 mL

* Corresponding author fax, 0032-16-321998; e-mail, Johan.Martens@agr.kuleuven.ac.be

10.1021/jp992272y CCC: $18.00
Published on Web 11/30/1999

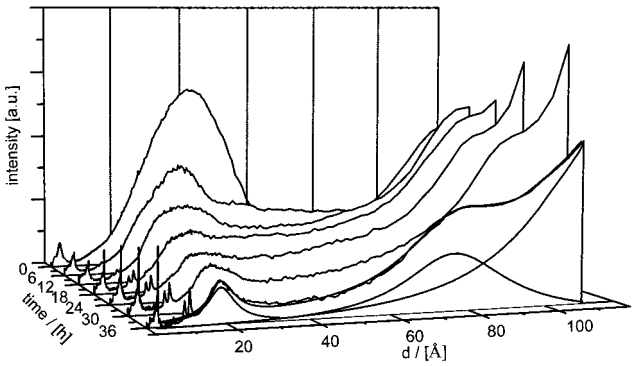

Figure 1. Measured X-ray pattern of the "closed" system as function of *d*-value and time, between 6 and 36 h at 373 K. With the pattern at 36 h the fitted curve consisting of three Lorentzians has been included.

aqueous tetrapropylammonium hydroxide (TPAOH; Fluka 40%) and 9 mL water for 2 h at room temperature.[1−3,12] Equal amounts of the nanoblock solution were transferred into two identical polypropylene bottles. One was screwed tight and kept in an oven heated to 373 K ("closed" system). The other bottle was fitted with a reflux heater and placed in a water bath ("open" system), also kept at 373 K.

The crystallization was followed using X-ray diffraction in a Debye−Scherrer configuration.[3] For the determination of the evolution of particle populations with time, at selected times small liquid samples were filled in capillaries with internal diameter of 1 mm and sealed.

The uncorrected low angle region of the diffraction data expressed as a function of the *d*-value for the closed system at different times is illustrated in Figure 1. The low angle region of all these diffractograms of the closed system as well as for the open system could be fitted by 1 to 3 Lorentzian lines[3] corresponding to 1 to 3 populations of differently sized particles. The size of the scattering entities was determined using the mathematical relationship between the diameter in space *D* and the position of the scattering *d* for a slab like particle[3]

$$d = D \times 0.64 \qquad (1)$$

The fitting of the X-ray patterns as a whole allowed also the size estimation for signals for which the maximum intensity occurred at angles too low to be observed ($d > 20$ nm, Figure 1; 36 h). The range of thus detectable particle sizes extends to *d*-values of ca. 30 nm.

The recorded intensity of each signal was normalized to allow determination of the particle populations on volume basis.[3] As normalization condition served the hypothesis that all of the silicon is present in scattering entities, as verified for the nanoslab suspension.[3] In the parent suspension, 70% of the silicon is present as nanoslabs; 30% as intermediates. The volume of the large particle fraction was estimated by difference when out of observation range.

The Bragg patterns were analyzed between 7 and 60° 2θ. Rietveld refinement with the GSAS software package[13] was used to determine the relative amount of crystalline material susceptible to Bragg diffraction,[14] as mirrored in the scaling factor. The refined data of the final colloidal Silicalite-1 product was taken as starting parameters[12] (Figure 2). The refinement was concerned with scaling factor, background parameters, and profile function only. The goodness of fit was checked by the reliability factors, determined by comparing calculated and measured structure factor (Rf), and diffraction profile (Rp and Rwp). The Rf factors were throughout below 11%, with Rp and Rwp ranging between 2 and 3% and 3 and 4%, respectively.

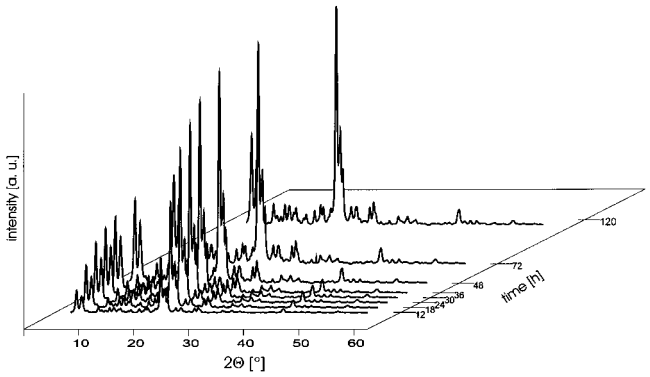

Figure 2. Rietveld refined X-ray patterns of the "open" system, used to obtain the volume of Bragg crystalline material.

TABLE 1: Measured Intensity (int) and Position (as *d*-value and 2Θ) of the Three Populations of Particles (nanoslabs, intermediates, and large particles) in the "Closed" System[a]

time/[h]	int/[%]		*d*/[Å]		2Θ/[°]		size of model/[Å]		
	Bragg	l.a.	obs	calc	obs	calc	*a*	*b*	*c*
				Nanoblocks					
0		66.2	37.68	37.15	2.35	2.38	13	40	40
6		20.6	36.44		2.43				
12		13.2	29.69	29.81	2.98	2.97	13	40	20
18		4.5	26.67	27.67	3.32	3.20	13	40	10
24		2.2	26.58		3.33				
30		1.3	19.60	20.04	4.52	4.42	13	26.7	10
36		1.0	19.59		4.52				
				Intermediates					
0		27.7	116.48	116.70	0.76	0.76	143	80	80
6		83.2	108.97		0.81				
12		76.5	106.35	110.30	0.83	0.80	130	80	80
18		57.2	102.64		0.86				
24		34.8	97.00	98.35	0.91	0.90	104	80	80
30		17.1	90.07		0.98				
36		7.9	78.90	79.69	1.12	1.11	52	80	80
48		1.6	67.90		1.30				
72		1.4	64.17	66.21	1.38	1.34	52	80	40
120		0.3	56.68	57.84	1.56	1.53	13	80	40
				Large Particles					
0	0.0	0.0							
6	0.0	1.3	144.70	146.57	0.61	0.60	143	160	80
12	4.7	3.8	208.18	206.05	0.43	0.43	143	240	160
18	39.3	31.9	280.51	303.75	0.32	0.29	143	320	320
24	74.3	63.1	>300						
30	90.2	81.6	>300						
36	96.7	91.1	>300						
48	99.0	98.4	>300						
72	99.7	98.7	>300						
120	100.0	99.7	>300						

[a] Intensity has been derived as Bragg intensity and from low angle scattering (l.a.). The position of the signals (obs) is compared to calculated (calc) values, based on the aggregation model.

The evolution with time of the refined XRD patterns of the closed system is shown in Figure 2. The Bragg patterns were not analyzed for line broadening, because first the intensity of the reflections was too low for detailed particle size analysis and later the resolution of the diffractometer did not suffice.

Results and Discussion

Crystallization Kinetics of Colloidal Silicalite-1 in an Open and Closed System. The XRS at low angles gave evidence for the existence of particle populations with discrete sizes all along the two crystallization processes studied. Acquired X-ray data and assignments are summarized in Tables 1 and 2. For the rationalization of the low angle XRS data, it is convenient to assign the three signals to (1) nanoslabs ($d_{obs} \leq 3.7$ nm); (2) intermediates (5.7 nm $< d_{obs} <$ 13 nm); and (3) large particles

TABLE 2: Measured Intensity (int) and Position (as *d*-value and 2Θ) of the Three Populations of Particles (nanoslabs, intermediates, and large particles) in the "Open" System[a]

	int/[%]		d/[Å]		2Θ/[°]		size of model/[Å]		
time/[h]	Bragg	l.a.	obs	calc	obs	calc	*a*	*b*	*c*
				Nanoblocks					
0		72.9	37.68	37.15	2.35	2.38	13	40	40
1		71.4	38.51		2.30				
2		64.1	36.88		2.40				
3		55.4	37.91		2.33				
6		43.8	37.28		2.37				
9		36.3	36.11		2.45				
12		31.2	35.07		2.52				
15		27.6	34.16		2.59				
18		23.4	33.06	33.06	2.68	2.68	13	40	30
24		17.5	30.77		2.88				
27		15.1	29.29	29.81	3.02	2.97	13	40	20
30		13.5	28.47		3.11				
32		12.5	27.10	27.67	3.27	3.20	13	40	10
36		10.1	26.78		3.31				
39		8.6	26.09		3.39				
41		7.2	25.25		3.51				
44		7.9	23.82		3.72				
46		7.1	23.05		3.84				
48		6.2	22.39		3.95				
60		4.5	19.90	20.04	4.45	4.42	13	26.7	10
70		3.4	18.56		4.77				
94		2.0	17.22		5.14				
				Intermediates					
0		29.8	116.48	113.05	0.76	0.78	143	80	80
1		31.1	117.60		0.75				
2		37.4	118.81	119.478	0.75	0.74	156	80	80
3		44.8	120.06		0.74				
6		54.8	120.18		0.74				
9		61.2	120.69		0.73				
12		65.5	122.03		0.73				
15		68.6	122.03		0.73				
18		72.1	122.03		0.73				
24		73.4	122.03		0.73				
27		70.9	122.03		0.73				
30		62.0	122.03		0.73				
32		51.0	121.00		0.73				
36		41.1	121.16		0.73				
39		28.5	121.74		0.73				
41		24.7	122.03		0.73				
44		16.3	122.03		0.73				
46		13.1	122.03		0.73				
48		12.0	122.03		0.73				
60		5.6	122.03		0.73				
70		4.6	122.03		0.73				
94		3.0	122.03		0.73				
				Large particles					
15	0.0	3.9	197.12	199.61	0.45	0.44	143	240	160
18	0.0	4.5	220.70	238.88	0.40	0.37	143	320	160
24	3.8	9.1	283.34	294.25	0.31	0.30	143	320	320
27	10.1	14.0	>300						
30	17.6	24.5	>300						
32	26.8	37.6	>300						
36	54.4	48.8	>300						
39	68.6	62.9	>300						
41	75.0	68.0	>300						
44	82.2	75.8	>300						
46	86.7	79.8	>300						
48	89.1	81.8	>300						
60	96.1	89.9	>300						
70	97.8	92.1	>300						
94	100.0	97.1	>300						

[a] Intensity has been derived as Bragg intensity and from low angle scattering (l.a.). The position of the signals (obs) is compared to calculated (calc) values, based on the aggregation model.

($d_{obs} \geq 14.5$ nm). All experimental *d*-values (d_{obs}) of intermediate and large particles are consistent with the presence of slabs with dimensions that are multiples of the nanoslabs (1.3 × 4 × 4 nm) (Tables 1−2).

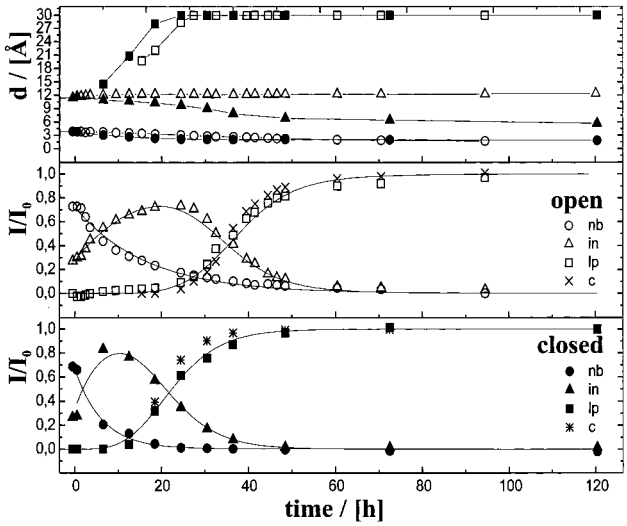

Figure 3. Evolution of particle populations in size and normalized scattering intensity. Nanoslabs (nb), intermediates (in), large particles (lp), and Bragg crystalline material (c) are represented by open symbols for the "open" system and filled symbols for the "closed" system. Particles larger than 30 nm were not analyzed for size. The continuous lines were calculated using the consecutive reaction model with the derived rate constants and autocatalytic exponent. As normalized starting concentrations for the numerical integration served $[nb]_0 = 0.6$ and $[lp]_0 = 10^{-10}$.

The evolution of the observed *d*-values and of the populations of nanoslabs, intermediates, and large particles in the course of Silicalite-1 crystallization in the open and the closed conditions is shown in Figure 3. The original size of the intermediates corresponds to a stacking of eleven square tablets of four nanoslabs, linked two-by-two through their small sides (14.3 × 8 × 8 nm, 44 nanoslabs, $d_{calc} = 11.7$ nm). This result matches closely the particle dimensions detected by Watson et al. using SAXS in a similar system.[5] Assuming cylindrical shape, those authors arrived at a diameter of 7.2 nm and a length of 14.1 nm. In comparison to our stack of tablets with $a = 14.3$ nm and $b = c = 8$ nm, the coincidence is very good.

In the open system, the size of the intermediates remains quite constant. The number of tablets in the stacking evolves from eleven to twelve. In the closed system, there is a gradual decrease in the number of tablets in the stacking. The size of the residual intermediates at the end of the crystallization corresponds to that of a half tablet (1.3 × 4 × 8 nm). In both systems, the size of the large particles quickly increases after their first observation to beyond the observation limit with low angle XRS.

In both systems in the first hours upon heating, the initial amount of nanoslabs of close to 70% decreases exponentially in favor of the intermediates. With time, the volume of intermediates goes through a maximum (Figure 3), heralding the onset of formation of large particles. As soon as these large particles were detected, Bragg scattering was observed, indicating the crystalline nature of these entities. In the open and the closed system, the Bragg crystallinity curve follows closely the volume of large particles as determined by low angle analysis (Figure 3). This can be taken as further evidence for the accuracy of the normalization procedure in the low angle region. It also justifies the distinction between intermediates and large particles, the latter consisting of the final crystalline product. The change of volumes of nanoslabs (nb), intermediates (in), and large particles (lp) with time resembles in both systems a pattern of consecutive reactions. The curves for the formation of the large particles display a clear induction period followed by a sigmoidal

TABLE 3: Initial Nanoslab Concentration, Rate Constants, and Autocatalytic Exponent Derived from Kinetic Analysis of the Data in Tables 1 and 2

	nb(0)	$k1/[h^{-1}]$	$k2/[h^{-1}]$	n
open	0.7	0.06	0.15	0.78
closed	0.62	0.12	0.16	0.68

shape, typical for an autocatalytic process (a.c.). The following kinetic scheme was adopted for modeling of the observed kinetics:

$$nb \xrightarrow{k1} in \xrightarrow[a.c.]{k2} lp \tag{2}$$

The measured data implied that the second reaction step is much faster at the investigated reaction temperatures around 373 K than the equilibration of nanoslabs and intermediates, so that the back reaction of intermediates into nanoslabs could be neglected. Unfortunately the autocatalytic behavior in the last step leads to nonlinear differential equations for the rate laws

$$\frac{\mathrm{d[nb]}}{\mathrm{d}t} = -k1[\mathrm{nb}] \tag{3}$$

$$\frac{\mathrm{d[in]}}{\mathrm{d}t} = k1[\mathrm{nb}] - k2[\mathrm{in}][\mathrm{lp}]^n \tag{4}$$

$$\frac{\mathrm{d[lp]}}{\mathrm{d}t} = k2[\mathrm{in}][\mathrm{lp}]^n \tag{5}$$

The decay of the volume of nanoslabs in the system (Figure 3) leads in a straightforward manner to the determination of k1 and the initial concentration of nanoblocks. To determine k2 and n, the derivative of lp(t) was numerically determined from the measured data and divided by in(t). Its logarithm yielded a straight line with n being the slope and ln(k2) the intercept. To check the validity of the constants thus determined, the rate laws for lp and in were numerically integrated, using a Katta−Runge method of fourth order. Comparison with the experimental data proves the good description of the mechanism by the determined rate constants (Table 3, Figure 3, continuous lines).

Nanoslab Aggregation and DLVO Theory. Several authors[4−10] reported the simultaneous observation of distinct populations of subcolloidal and colloidal particles throughout crystallization processes of Silicalite-1. As a possible crystallization mechanism, Schoeman proposed the dissolution of part of the subcolloidal particles to provide a nutrient reservoir for the growth.[4] Schoeman's model was based on an estimation of the interaction potential between the subcolloidal and colloidal species, assuming a spherical particle shape with homogeneous surfaces interacting. These calculations resulted in very high energy barriers for the approach of particles larger than 7 nm, arguing against a growth by aggregation.

The assumptions of Schoeman's model are less adequate in view of the present knowledge on the nature of the subcolloidal particles, being the nanoslabs (Figure 4). They have slab-like rather than spherical geometry and an MFI-like structure with occluded TPA molecules. The presently proposed consecutive aggregation mechanism not involving dissolution more easily accounts for the simultaneous presence of a nanoslab fraction, intermediately sized entities, and a population of growing large particles.

For the nanoslabs, the potential energy as a function of interparticle distance was calculated based on the extended

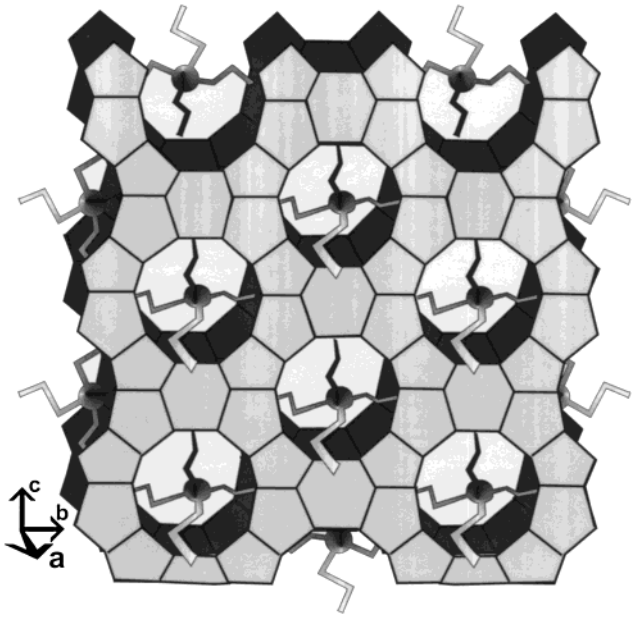

Figure 4. Schematic representation of a nanoblock with included templates.

DLVO theory[4,15,16] to decide whether the blockwise aggregation is energetically feasible or not. The potential energy consists of four terms,[4] the van der Waals attraction, the repulsion stemming from interaction of the charged double layers, steric repulsion due to interaction of surface attached groups, and solvation energy. Each contribution was determined in units of kT, allowing comparison of available thermal energy with the barrier to overcome.

$$\frac{E_{\mathrm{pot}}}{kT} = \frac{E_{\mathrm{vdw}}}{kT} + \frac{E_{\mathrm{rep}}}{kT} + \frac{E_{\mathrm{ster}}}{kT} + \frac{E_{\mathrm{solv}}}{kT} \tag{6}$$

The solvation energy is known to be at least 2 orders of magnitude lower than the other terms[4,15,16] and has not been taken into account. The expressions derived for flat surfaces have been selected,[15,16] and the total potential energy was calculated (see Supporting Information). At all distances r, the van der Waals attraction is larger than the repulsive Coulombic potential of the double layers of two interacting flat surfaces, as discussed by Schoeman for spherical particles.[4] Therefore, steric repulsion is responsible for the stabilization of the observed colloidal and subcolloidal entities. For this reason, the parameters for the calculation of this contribution have to be selected with great care. The steric repulsive energy in units of kT and per unit area a can be expressed as a function of the coverage per area τ and the effective size of the part of the molecule being exposed on the surface, the headgroup size L,

$$\frac{E_{\mathrm{ster}}}{akT} = \frac{100\tau^{3/2}L}{\pi}\,\mathrm{e}^{\frac{-\pi r}{L}} \tag{7}$$

Equation 7 was derived for polymeric chains firmly attached to a given surface.[15,16] Considering the nanoslabs in which TPA cations are partially included in cages and pointing with one alkyl chain toward the liquid phase (Figure 4), this is not too far off the mark. The coverage can then be calculated with the observed number of surface-adsorbed TPA molecules determined by thermogravimetry and the knowledge of the detailed nanoslab structure.[1−3] It turned out that approximately all of the cages and halfcages formed on the outer surfaces of the nanoslab (Figure 4) are occupied with TPA molecules.[1] Due to

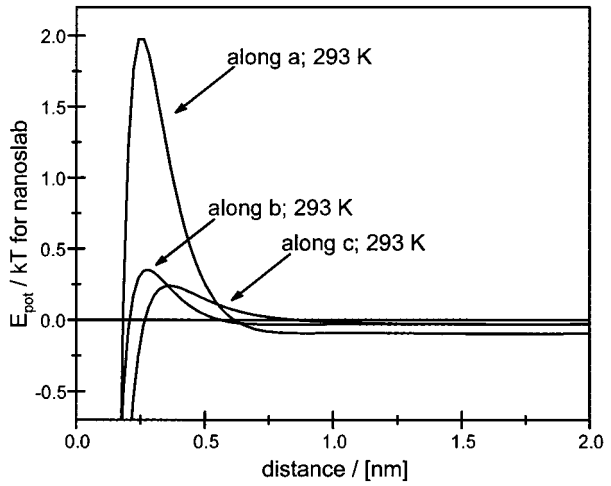

Figure 5. Potential energy per thermal energy as function of surface distance of a nanoslab (perpendicular to its crystallographic directions *a*, *b*, and *c*) toward a similar surface at room temperature.

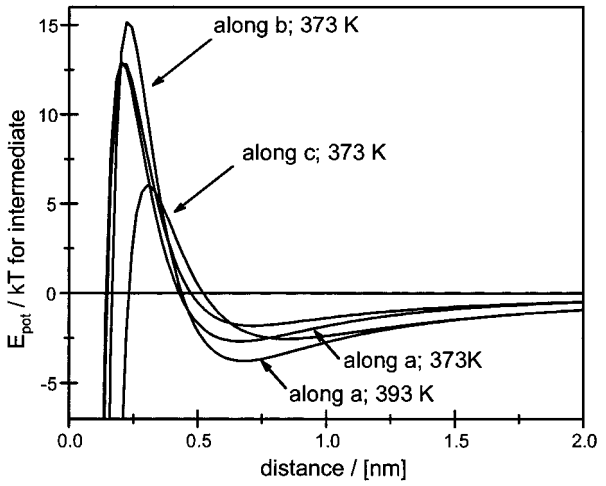

Figure 6. Potential energy per thermal energy as function of surface distance of an intermediate (perpendicular to its crystallographic directions *a*, *b*, and *c*) toward a similar surface at 373 K. Also included is the energy function for approach perpendicular to *a* at 393 K.

the specific structure of the slab, this implies different surface properties in the three different crystallographic directions. Therefore, the aggregation rates in the different directions are expected to be different. For Silicalite-1, differences in crystal growth rate in the different crystallographic directions have been observed.[17−19]

Inspection of Figure 4 illustrates the decoration of the three sides by alkyl chains. From the largest surface of 4 × 4 nm^2, perpendicular to the sinusoidal channels and perpendicular to the *a* direction, six alkyl chains protrude. Each belongs to a template ion in one of the six fully formed cavities. The number of TPA^+ and extended propyl groups, respectively, on the smaller sides of the slab is two perpendicular to the straight channels running in the *b* direction and even less (between one and two) perpendicular to the *c* direction. Accounting for the flexibility of the propyl chains, an effective headgroup size of 0.5 nm was assumed for the plane perpendicular to *c*. The planes perpendicular to the sinusoidal and straight channels are strongly puckered with the templates residing in deep pockets. Consequently, a smaller headgroup size of 0.4 nm was assumed. The resulting potential energies at 293 K (room temperature) as function of interparticle distance for all three sides of the nanoslab are presented in Figure 5. The energy barriers in the *b* and *c* directions are small. There is some attraction of the nanoslabs when they approach each other with their large faces (along the *a* direction), but the barrier at close distances is considerable.

The intermediates observed at room temperature[3] as well as at the crystallization temperature (Tables 1 and 2) are stacks in the *a* direction of variable numbers of thin sheets of 2 × 2 nanoslabs linked in the *b* and *c* directions. The energy profiles for the approach of a nanoblock toward a similar surface (Figure 5) suggest that these intermediates can have chemical linkage in the *b* and *c* direction, through the small sides of the nanoslab, and physical linkage along *a*. The enlarged surfaces of the *ac* and *bc* faces in intermediates compared to the nanoslab lead to an increased repulsive force between approaching particles so that no further aggregation at room temperature along *b* or *c* takes place. This explains the presence of a discrete population of intermediates along with still present nanoslabs at room temperature.

The results of the calculations of the potential energy between two intermediates consisting of twelve stacks of square tablets (48 nanoslabs), approaching a similar surface in the *a*, *b*, and *c* directions at 373 K, are shown in Figure 6. This situation is representative for the fusion of the tablets in the intermediates and the subsequent formation of large particles. Compared to the nanoslabs at 293 K (Figure 5), the energy barriers have increased, due to the increase of temperature and size of the aggregating species. On first sight this should prevent further crystallization. It is noteworthy, however, that the potential energies as a function of approach in all directions display minima at a distance of about 0.75 nm. The depths of these wells are in the order of the thermal energy of the particles. Therefore, the slabs do not only approach but remain physically trapped next to each other. Thus they have the time to assume the correct orientation necessary for the silicon condensation. The barriers calculated using the extended DLVO theory do not account for these rearrangements of the interacting surfaces. Therefore, this model is valid only at distances larger than a critical value where these rearrangements, driven by mutual interactions of adsorbed templates and silicate surfaces, can take place. After alignment, the maximization of an inner hydrophobic surface for interaction with the included template molecules has to be considered[20] as a driving force. At a certain point during the approach of the particles, this effect takes over and facilitates first the alignment and then the fusion of the adjacent surfaces. The minima of potential energy for the different approaches, calculated with the DLVO theory, grant the trapped particles sufficient time for assuming the right orientation of their faces. This accounts for the observation of coaxial fusing of the intermediate particle population, which has also been reported before.[3,5] As the lowest energy barrier is encountered along *c* (Figure 6), the fusion of intermediates will preferably take place in this direction, which has already been identified as the preferred growth direction of Silicalite-1.[21−23]

To gain some insight into the effect of the temperature on the aggregation mechanism, the potential energy for the approach of an intermediate along *a* has been calculated also at 393 K (Figure 6). The minimum in the energy profile is lower at 393 K compared to 373 K, whereas the height of the barrier remains approximately the same (Figure 6). This accounts for the acceleration of the crystallization with temperature.

Influence of Synthesis Conditions. It is curious that the open and closed systems vary markedly in the observed rate constants despite similar reaction temperatures. Two differences during crystallization can be responsible for this discrepancy: convec-

tion and concentration. In the open system a larger amount of solvent is in the gas phase. Therefore, the concentration of siliceous particles is slightly higher than in the closed system. In a series of experiments where increasing amounts of solvent were removed, the rate of both aggregation steps (eq 2) was found to increase with increasing concentration. If the difference in concentration had played a role in the presently described systems, the open system should therefore have aggregated faster than the closed one. Instead, we detected a retarded formation of intermediates in the open system compared to the closed environment.

The reflux arrangement caused more turbulence due to dripping and temperature gradients. Therefore, in the closed system, convection was reduced in comparison to the open system. The formation of intermediates involves stacking of sheets along *a*. The formation of the chemical bonds is preconditioned by ordering of the orientation of the connecting surfaces and, most importantly, of the alkyl chains sticking out. This slow process is expected to be favored by reduction of the dynamics to prevent the particles from being prematurely ripped apart. This explains the higher value for the rate constant $k1$, defining the formation of intermediates, in the closed system (Table 3). In additional experiments with intentional agitation with a magnetic stir bar, the onset of the formation of large particles was found to be even more retarded. The liquid turned turbid only after 5 days, whereas the closed system already was fully opaque after only 12 h. This supports the reasoning that the aggregation of particles along *a* depends considerably on the convection conditions in the system. This difficulty to align perfectly before fusion also explains the previously observed strain in this direction in the final product.[12]

On the other hand, aggregation of the intermediates, especially along *c*, should not be severely affected by convection. The *ab* plane contains only very weakly bound templates because only part of the cages is formed. Ordering, therefore, should occur easily and quickly. Consequently, the effect of convection should not be too extensive during the formation of large particles, as expressed in the similarity of the rate constants $k2$ for the open and closed system (Table 3).

Despite the fact that the aggregation mechanisms of intermediates in open and closed systems are occurring at almost the same rate, the autocatalytic behavior in the open system is more pronounced. In terms of the proposed aggregation mechanism (Figure 7), column-like intermediates obtained by stacking of up to twelve sheets of four nanoslabs along *a* aggregate to give larger particles. Our DLVO calculations indicate that time for the necessary ordering process before the fusion of intermediates is granted because minima in potential energy exist at surface distances of about 0.75 nm. Considering now regular blocks successively attaching to large particles, it is plausible to assume that the large particles contain faults where the intermediates were not tightly packed and correctly bonded. Upon colliding, these large particles can break along the weak layers where the bonds are mainly physical, increasing therewith the preorganized surface of the large particle fraction suitable for addition of intermediates. It can account for the observed autocatalytic behavior. Increased convection favors the breaking apart of imperfect larger particles accounting for the observation of the steeper curve of formation of large particles in the open system (Figure 3).

Conclusions

The progress of crystallization of colloidal Silicalite-1 with TPA as template in the open and closed system for a given composition and temperature can be accurately described at the molecular level and kinetically modeled. At room temperature nanoslabs with dimensions of $1.3 \times 4 \times 4$ nm are formed, where the large 4×4 nm^2 surface is perpendicular to *a*. These nanoslabs form already at room temperature thin sheets linked via the small sides in the *b* and *c* direction. Due to stability criteria, the thin 2×2 sheets first have to stack in the *a* direction to give mechanically more stable blocks (intermediates) which then can be built into larger particles. But, at room temperature, further aggregation is energetically unfavorable. The equilibrium between nanoslabs and intermediates is shifted toward the right by a rise of temperature to 373 K. The potential energy of the intermediates as a function of interparticle distance has a minimum at about 0.75 nm. The intermediates can now prearrange before binding. Because of the propyl chains extending from the surfaces, the intermediates aggregate in a less ordered fashion to give the fraction of large particles. Upon colliding, several larger particles again break apart where stacking faults were introduced. This increases the amount of preorganized surface suitable for irreversible binding of intermediates. This model derived from extended DLVO theory accounts for the observed autocatalytic formation of the large particles. Growth along *c* involves the lowest energy barriers, explaining the growth rates and shapes of Silicalite-1 crystallites determined by others.

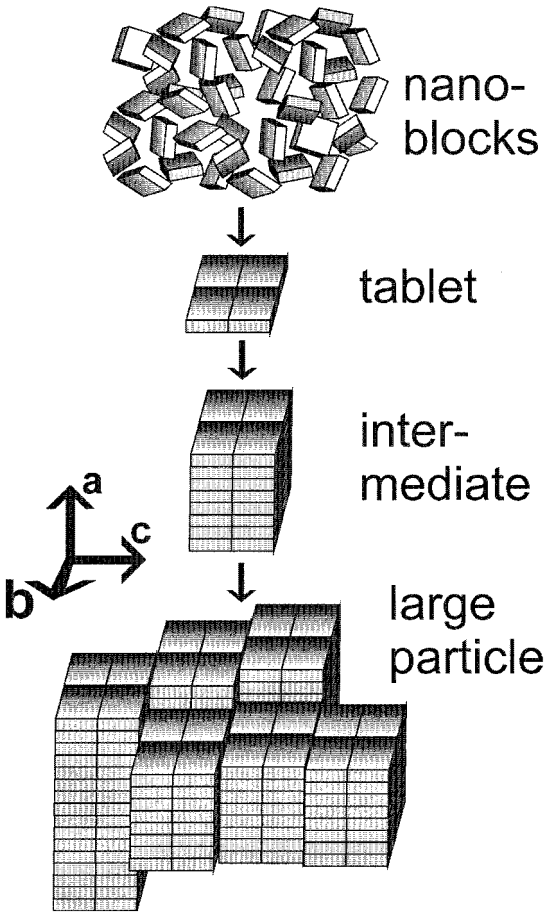

Figure 7. Schematic representation of the formation of Silicalite-1 material from clear solutions at elevated temperatures.

Regarding particle sizes, the presented mechanism covers the model proposed by Watson et al.[5] But, aside from the sole definition of particle sizes present in the course of crystallization, it can explain the observed differences in the rate constants depending on synthesis conditions.

Acknowledgment. This work was performed with financial support from the Belgian government (IUAP-PAI program) and the Flemish government through the FWO Vlaanderen. C.E.A.K. acknowledges the IUAP, and R.R. the K.U.Leuven for a postdoctoral fellowships.

Appendix

Constants and Values for DLVO Calculations. Calculations were based on the formula (see Supporting Information)

$$\frac{E_{tot}}{kT} = a\left(\frac{-A}{kTr^2 12\pi} + \frac{64n_\infty\gamma_0^2}{\kappa}\,e^{-\kappa r} + \frac{100\tau^{3/2}L}{\pi}\,e^{-\pi r/L}\right)$$

A is the Hamaker constant describing the strength of van der Waals interaction: 0.651×10^{-20} J.[4,16]

n_∞ is the bulk concentration of ionic species: 3.75 m^{-3} [4].

Y_0 is the effective potential energy at the Stern layer, based on the Stern potential $\psi_s = -15 \times 10^{-3}$ V[4]. Y_0(293 K) = 0.1475; Y_0(373 K) = 0.1162; Y_0(393 K) = 0.1103.

κ is the reciprocal thickness of the double layer, based on the dielectric constant of a given medium and given temperature. κ(293 K) = 1/0.5 nm with ϵ(H_2O, 293 K) = 78.54, ϵ(EtOH, 293 K) = 24.3, and ϵ(293 K) = 69.2;[24] κ(373 K) = 1/0.4 nm with ϵ(H_2O, 373 K) = 55.7, ϵ(EtOH, boiling) = 17.8, and ϵ(373 K) = 49.2;[4,24] κ(393 K) = 1/0.25 nm with ϵ(H_2O, boiling) = 55.7, ϵ(EtOH, boiling) = 17.8, and ϵ(393 K) = 49.2.[24]

τ is the coverage of particles by "grafted hairs". $\tau(\perp a)$ = 0.375/nm^2; $\tau(\perp b)$ = 0.384/nm^2; $\tau(\perp c)$ = 0.288/nm^2.

L is the length of the headgroup. $L(\perp a) = L(\perp b)$ = 0.4 nm; $L(\perp c)$ = 0.5 nm.

Supporting Information Available: Total potential energy calculations for the expressions derived for flat surfaces. This material is available free of charge via the Internet at http://pubs.acs.org.

References and Notes

(1) Ravishankar, R.; Kirschhock, C. E. A.; Knops-Gerrit, P.-P.; Feijen, E. J. P.; Grobet, P. J.; Vanoppen, P.; De Schryver, F. C.; Miehe, G.; Fuess, H.; Schoeman, B. J.; Jacobs, P. A.; Martens, J. A. *J. Phys. Chem. B* **1999**, *103*, 4960.

(2) Kirschhock, C. E. A.; Ravishankar, R.; Verspeurt, F.; Grobet, P. J.; Jacobs, P. A.; Martens, J. A. *J. Phys. Chem. B* **1999**, *103*, 4965.

(3) Kirschhock, C. E. A.; Ravishankar, R.; Looveren, L. V.; Jacobs, P. A.; Martens, J. A. *J. Phys. Chem. B* **1999**, *103*, 4972.

(4) Schoeman, B. J. *Microporous and Mesoporous Materials* **1998**, *22*, 9.

(5) Watson, J. N.; Iton, L. E.; Keir, R. I.; Thomas, J. C.; Dowling, T. L.; White, J. W. *J. Phys. Chem. B* **1997**, *101*, 10094.

(6) Schoeman, B. J.; Regev, O. *Zeolites* **1996**, *17*, 447.

(7) Schoeman, B. J. *Zeolites* **1997**, *18*, 97.

(8) Twomey, T. A. M.; Mackay, M.; Knipers, H. P. C. E.; Thomson, R. W. *Zeolites* **1994**, *14*, 162.

(9) Beelen, T. P. M.; Dokter, W. H.; van Garderen, H. F.; van Santen, R. A. In *Synthesis of Porous Materials, Zeolites, Clays, and Nanostructures*; Occelli, M. L., Kessler, H., Eds.; Dekker Inc.: New York 1997; p 59.

(10) Regev, O.; Cohen, Y.; Kehat, E.; Talmon, Y. *Zeolites* **1994**, *14*, 314.

(11) Keijsper, J. J.; Post, M. F. M. In *Zeolite Synthesis*, ACS Symposium Series 398, Occelli, M. L., Robson, H. E., Eds.; American Chemical Society: Washington, D.C., 1989; p 28.

(12) Ravishankar, R.; Kirschhock, C.; Schoeman, B. J.; Vanoppen, P.; Grobet, P. J.; Storck, S.; Maier, W. F.; Martens, J. A.; De Schryver, F. C.; Jacobs, P. A. *J. Phys. Chem. B* **1998**, *102*, 2633.

(13) Larson, A. C.; Von Dreele, R. B. *GSAS, General Structure Analysis System, Report LAUR 86*, Los Alamos National Laboratory: New Mexico, 1995.

(14) Jacobs, P. A.; Derouane, E. G.; Weitkamp, J. J. C. S. *Chem. Commun.* **1981**, 591.

(15) Hiemenz, P. C.; Rajagopalan, R. *Principles of Colloid and Surface Chemistry*, 3rd ed.; Marcel Dekker: New York, 1997.

(16) Israelachvili, J. N. *Intermolecular and Surface Forces*, 2nd ed.; Academic Press: London, 1991.

(17) Cundy, C. S.; Henty, M. S.; Plaisted, R. J. *Zeolites* **1995**, *15*, 342.

(18) Cundy, C. S.; Henty, M. S.; Plaisted, R. J. *Zeolites* **1995**, *15*, 353.

(19) Feoktistova, N. N.; Zhdanov, S. P.; Lutz, W.; Bülow, M. *Zeolites* **1989**, *9*, 136.

(20) Burkett, S. L.; Davis, M. E. *J. Phys. Chem.* **1994**, *98*, 4647.

(21) Jansen, J. C.; Engelen, C. W. R.; van Bekkum, H. In *Zeolite Synthesis*, ACS Symposium Series 398; Occelli, M. L., Robson, H. E., Eds.; American Chemical Society: Washington, D.C. 1989; p 257.

(22) Iwasaki, A.; Hirata, M.; Kudo, I.; Sano, T.; Sugawara, S.; Ito, M.; Watanabe, M. *Zeolites* **1995**, *15*, 308.

(23) Iwasaki, A.; Hirata, M.; Kudo, I.; Sano, T. *Zeolites* **1996**, *16*, 35.

(24) *Handbook of Chemistry and Physics*, 60th ed.; CRC Press: Boca Raton, FL, 1981.